Langmuir

Article

pubs.acs.org/Langmuir

Kinetics of Surfactant Desorption at an Air−Solution Interface

C. E. Morgan,[†] C. J. W. Breward,[†] I. M. Griffiths,[†] P. D. Howell,[†] J. Penfold,*[,‡,§] R. K. Thomas,[‡] I. Tucker,[⊥] J. T. Petkov,[⊥] and J. R. P. Webster[§]

[†]Mathematical Institute, University of Oxford, 24-29 St. Giles, Oxford OX1 3LB, United Kingdom

[‡]Physical and Theoretical Chemistry Laboratory, University of Oxford, South Parks Road, Oxford OX1 3QZ, United Kingdom

[§]ISIS Facility, STFC, Rutherford Appleton Laboratory, Chilton, Didcot, OXON, OX11 0QX, United Kingdom

[⊥]Unilever Research and Development Laboratory, Port Sunlight, Quarry Road East, Bebington, Wirral, United Kingdom

ABSTRACT: The kinetics of re-equilibration of the anionic surfactant sodium dodecylbenzene sulfonate at the air−solution interface have been studied using neutron reflectivity. The experimental arrangement incorporates a novel flow cell in which the subphase can be exchanged (diluted) using a laminar flow while the surface region remains unaltered. The rate of the re-equilibration is relatively slow and occurs over many tens of minutes, which is comparable with the dilution time scale of approximately 10−30 min. A detailed mathematical model, in which the rate of the desorption is determined by transport through a near-surface diffusion layer into a diluted bulk solution below, is developed and provides a good description of the time-dependent adsorption data. A key parameter of the model is the ratio of the depth of the diffusion layer, H_c, to the depth of the fluid, H_f, and we find that this is related to the reduced Péclet number, Pe^*, for the system, via $H_c/H_f = C/Pe^{*1/2}$. Although from a highly idealized experimental arrangement, the results provide an important insight into the "rinse mechanism", which is applicable to a wide variety of domestic and industrial circumstances.

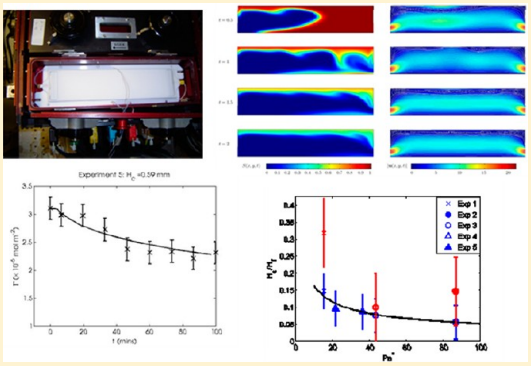

INTRODUCTION

The kinetics of surfactant adsorption are important in the context of foamability (formation of foams and lathers), foam and emulsion stability, wettability, and biological function (such as airway opening) and have been extensively studied and reviewed.[1−5] In all these areas, dynamic as well as equilibrium surface properties are of key importance. Dynamic measurements of surface tension provide access to the surface kinetics and have been extensively undertaken.[5,6] A variety of different approaches to the measurement of dynamic surface tension have been developed and include techniques such as drop volume, maximum bubble pressure, and pendant drop measurements.[4−6] These classical methods are now often automated[7,8] and are supplemented by techniques such as ellipsometry[9,10] that measure the kinetics of adsorption directly. More recently much attention has focused on the overflowing-cylinder geometry, which in combination with ellipsometry and neutron reflectivity (NR) has been used to probe the dynamics of surfactant adsorption.[11−13]

A number of detailed mathematical models exist for the description of dynamic surface tension and adsorption. The models can usually be considered as a two-stage process in which (i) molecules adsorb at the surface from a thin subsurface layer and (ii) bulk mass transfer (described by diffusion) occurs between the solution and the subsurface layer. A variety of different approaches have been proposed to model the diffusion process mathematically,[4,14] and often such descriptions give rise to the well-known Ward−Tordai equation.[15] Diamant et al.[16] used a free energy approach to derive a model similar to the Ward−Tordai equation to describe the kinetics of surfactant adsorption. In the diffusion-controlled model the adsorption process is considered to be instantaneous, while treatments that assume that the adsorption is not instantaneous, such as kinetic-controlled or mixed diffusion/kinetic-controlled models, have also been developed.[6,17] Tiberg et al.[9,10] have developed a model to describe the mass-transfer kinetics of adsorption and desorption at hydrophilic and hydrophobic surfaces after dilution of the subphase. Their model assumes that the dilution occurs instantaneously and so the adsorption process is controlled by diffusive transport through a stagnant layer at the surface. The model takes into account the formation and dissolution of micelles within the stagnant layer and the free energy of interaction of monomers and micelles with the surface.

Predominantly, studies of the dynamic surface tension using ellipsometry/NR using the overflowing cylinder have focused on the dynamics of surfactant adsorption. However, some studies have considered specifically the desorption process[8] or both adsorption and desorption.[7,9,10] The desorption process is particularly important in the context of the "rinse mechanism",

Received: October 15, 2012
Revised: November 19, 2012
Published: November 20, 2012

   dx.doi.org/10.1021/la304091g | *Langmuir* 2012, 28, 17339−17348

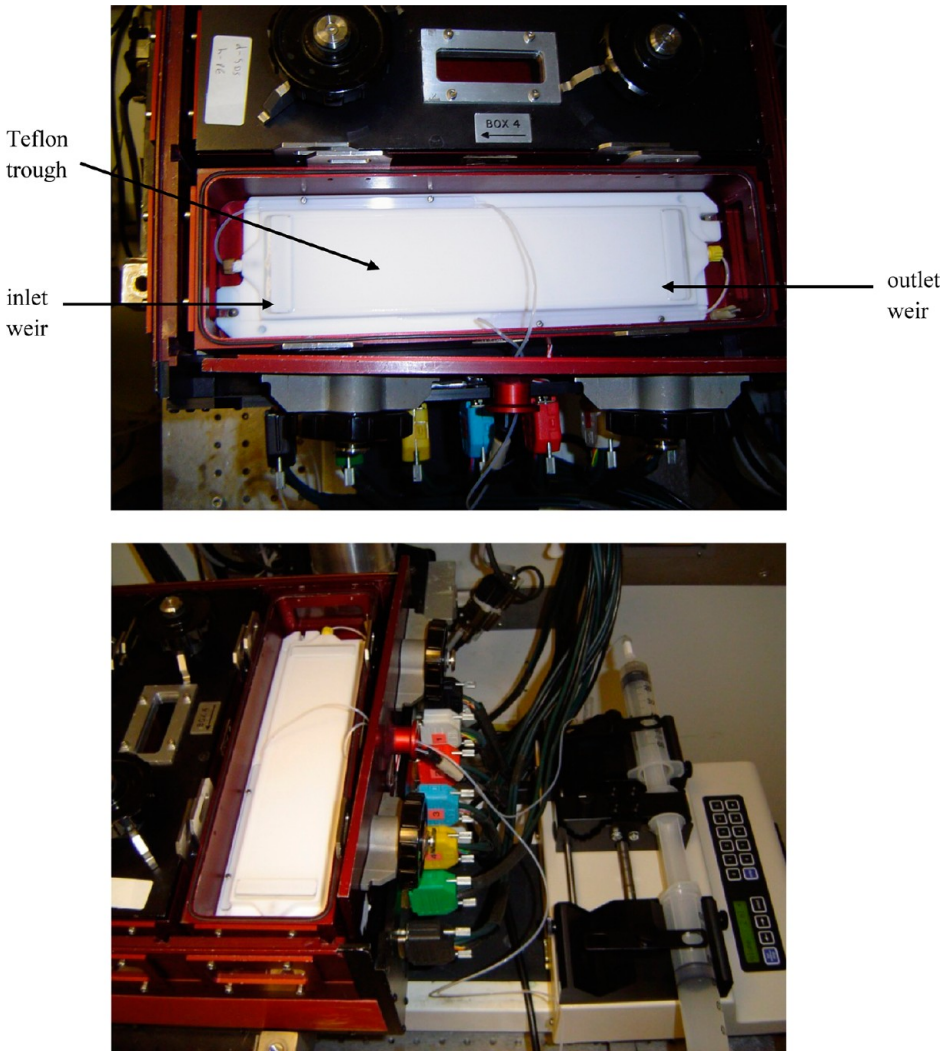

Figure 1. View of flow cell and its arrangement on the INTER beamline at ISIS.

i.e., the removal of detergent/soap in many home and personal care products,[18] and is a key element of their effectiveness. In this respect, most of the major manufacturers have sustainability programs in which reduced water usage is a major objective, motivating the need for more effective rinsing mechanisms. For example, Unilever aimed to reduce water usage in their product production and life cycles by 65% by 2009.[19] Hence, understanding the kinetics of desorption is important in terms of optimizing rinsing mechanisms. The focus of this paper is to explore the desorption of surfactants from a planar air−solution interface following the dilution of the subphase. The aim of the experiments is to provide insight into the mechanism and time scales associated with surfactant desorption. The measurements made here are for the simplest model for a hydrophobic interface and a highly idealized flow geometry, yet they provide a good initial starting point from which to develop a more detailed understanding.

It has been previously shown that NR, in combination with D/H isotopic substitution, is a powerful tool for studying surfactant adsorption at the air−solution interface.[20] In the context of such measurements, the ability to determine absolutely adsorbed amounts is a major advantage. Furthermore, the current generation of neutron instrumentation[21] is such that measurements can now be made in a few minutes, and thus on a time scale relevant to the kinetics of desorption. In combination with the NR measurements, a novel flow cell has been developed, in which the subphase can be exchanged (diluted) by a laminar flow while the surface region remains unaltered. To support and explain the NR measurements, we have developed a mathematical model in which the time dependence of the desorption is determined by diffusion from a near-surface stagnant layer into a diluted bulk solution below. Measurements have been made in null reflecting water (nrw) using deuterium-labeled sodium dodecylbenzene sulfonate, LAS-4. The solutions were diluted through the critical micelle concentrations (cmc). Measurements with different flow-cell geometries (different dimensions), flow rates, and dilution factors provide a detailed comparison between theory and experiment.

EXPERIMENTAL DETAILS

(i). Flow Cell. The flow cell and its arrangement on the INTER beamline[21] are shown in Figure 1. The Teflon trough (cell) is contained in an airtight box and is similar to the standard static air−water troughs used extensively elsewhere.[22] The Teflon trough incorporates a stainless-steel weir at each end, which is connected to a World Precision Instruments SP210/CZ push−pull syringe pump. Two different trough sizes were used, which provided a variation in the height of the weir relative to the total depth of the solution and in the

dx.doi.org/10.1021/la304091g | *Langmuir* 2012, 28, 17339−17348

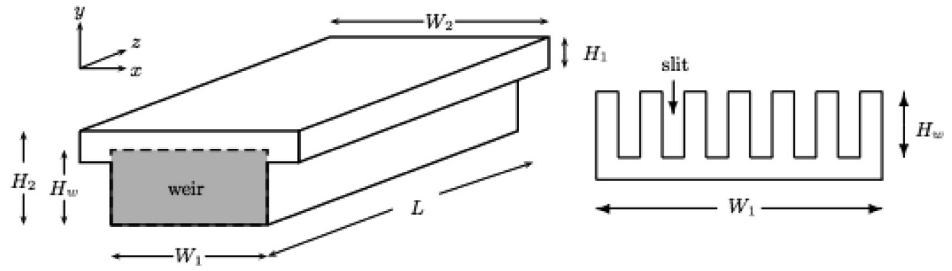

Figure 2. Schematic diagram of the trough and flow cell weir.

total solution volume (and hence the available dilution factor). The key dimensions and parameters are shown in Figure 2 and summarized in Table 1.

Table 1. Key Dimensions and Parameters for the Flow Troughs

trough size	W_1 (mm)	W_2 (mm)	H_1 (mm)	H_2 (mm)	L (mm)	H_w (mm)	total volume (mL)
large	50	53	1	2	216	1.5 (small)	30
small	50	53	1	4	70	3.0 (large)	25
small	50	53	1	2	70	1.5 (small)	15

Using the matched push−pull syringe pump, the subphase can be exchanged to dilute the bulk solution without altering the surface, and the flow rates can be varied from 0 to 10 mL/min. NR measurements, where D_2O in the trough was exchanged with itself, showed no change in the observed reflectivity. Furthermore, replacing a 2 mM d-LAS-4/nrw solution with the same solution also showed no change in the adsorption.

Figure 3 shows a flow profile for the experiment, obtained by solving the Navier−Stokes equations for an incompressible Newtonian

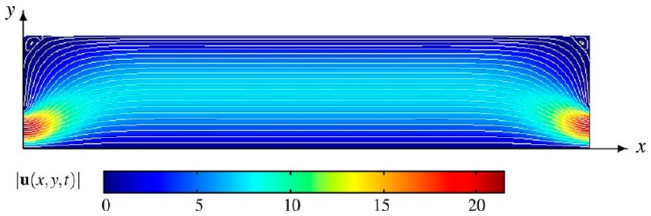

Figure 3. Flow pattern for trough, calculated using the COMSOL Multiphysics package.

fluid with a Poiseuille flow prescribed at the inlet boundary and zero pressure at the outlet boundary, using the COMSOL Multiphysics version 4.3 package with typical parameter values that are discussed in the Mathematical Model section of this paper. The calculation considers the flow profile in the *xy*-plane and assumes this profile is equivalent for each cross section for given values of *z*. The calculations show that, apart from a small region in the immediate vicinity of the entrance and exit weirs, the flow pattern is consistent with laminar flow.

(ii). Neutron Reflectivity. The NR measurements were made on the INTER reflectometer[21] at the ISIS pulsed neutron source at Rutherford Appleton Laboratory, U.K. The measurements on INTER were made using a single detector, at a fixed grazing angle of incidence, θ, of 2.3° and a neutron wavelength, λ, ranging from 0.5 to 15 Å to provide a wave vector transfer Q ($=4\pi \sin\theta/\lambda$) range of 0.03−0.5 $Å^{-1}$. For air/water measurements in nrw (with the scattering length density of zero) on INTER, the absolute reflectivity was calibrated with respect to the direct beam and the reflectivity from a D_2O surface. In the kinematic approximation the specular reflectivity is related to the square of the Fourier transform of the scattering length density profile, $\rho(z)$, normal to the interface[19]

$$R(Q) = \frac{16\pi^2}{Q^2} \left| \int \rho(z) e^{-iQz} dz \right|^2 \quad (1)$$

where $\rho(z) = \sum_i n_i(z) b_i$, $n_i(z)$ is the number density of the *i*th nucleus, and b_i is the scattering length. In the NR measurements, $\rho(z)$ can be manipulated by using hydrogen (H)/deuterium (D) isotopic substitution (H and D have different neutron scattering lengths, -3.71×10^{-5} Å for H and 6.674×10^{-5} Å for D), and this has been extensively exploited at the air−water interface for a range of surfactants.[20] The NR measurements were made at the air−water interface for the combination of d-LAS-4/nrw. For this isotopic combination, the reflected signal arises only from the deuterium-labeled surfactant adsorbed at the interface. In the case of a monolayer of surfactant adsorption, the reflectivity can be adequately described by a single layer of uniform density, to provide a thickness d and a scattering length density ρ.[20] The amount of surfactant at the interface is then given by

$$A = \frac{\sum_i b_i}{d\rho} \quad (2)$$

where $\sum_i b_i$ is the scattering length of the adsorbed surfactant (for d-LAS-4 $\sum_i b_i = 3.48 \times 10^{-3}$ Å). The adsorbed amount is given by $\Gamma = A/N_A$, where N_A is Avogadro's number. The typical error in the area per molecule is of the order ±2 $Å^2$ (for an area per molecule of 50 $Å^2$).[20] However, the measurements here were made for ∼5−15 min per point, and so the error in the area per molecule is greater, ∼±5 $Å^2$.

(iii). Materials and Measurements Made. The LAS isomer, LAS-4, used in this study is asymmetric and is functionalized at the C_4 position, as shown in Figure 4.

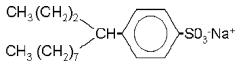

Figure 4. Structure of the LAS-4 surfactant used in this study.

The predeuterated LAS-4 was custom-synthesized at Oxford/Unilever R&D.[23,24] The purity of the LAS-4 was verified by surface tension and neutron reflectivity, and the values of the cmc was 1.6 mM, consistent with other reported measurements.[25] The measurements were all made at an initial surfactant concentration of 2 mM for the predeuterated surfactant in nrw and at a temperature of 25 °C. All glassware, pipe work, and Teflon troughs were cleaned in alkali detergent (Decon 90) and rinsed in copious amounts of high purity water. The experimental conditions for the different measurements are listed in Table 2 below. The different trough and weir sizes are listed in Table 1. Typical measurement times for the NR data were approximately 5−15 min per reflectivity profile, dependent upon the trough size.

(iv). Solution Concentration Measurements. For experiments 1−3 the concentration of the LAS-4 solution remaining in the flow trough after the initial dilution was determined separately using UV adsorption spectroscopy. The measurements were made using a Biolab GeneQuant 1300 UV visible spectrophotometer. A scan from 240 to

dx.doi.org/10.1021/la304091g | Langmuir 2012, 28, 17339−17348

Table 2. Summary of Experimental Conditions for the Different NR Measurements

exp. no.	surfactant	trough size	weir size	flow rate (mL/min)	volume exchange	no. of dilutions	time of dilution (min)
1	LAS-4	large	small	2.5	×2	3	24
2	LAS-4	small	small	2.5	×2	2	12
3	LAS-4	small	small	1.25	×4	1	48
4	LAS-4	small	small	0.625	×2	2	48
5	LAS-4	small	large	0.625	×2	2	80

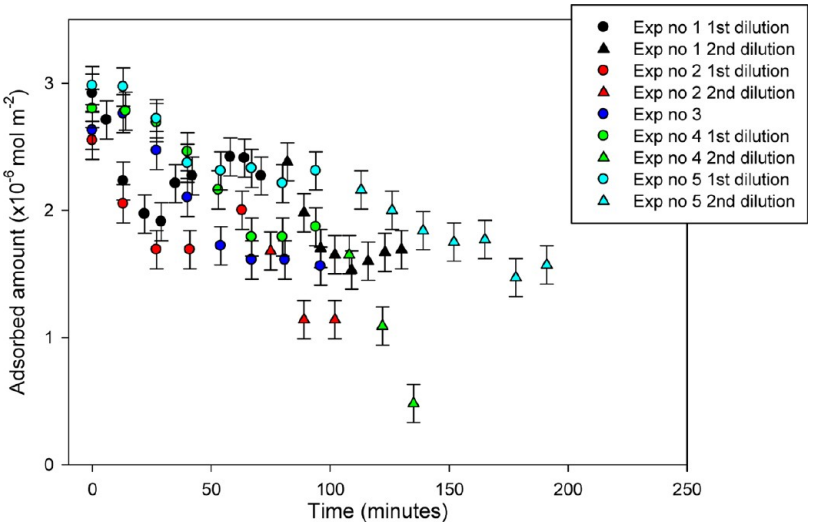

Figure 5. Time evolution of the adsorbed concentration for the five different experiments with the experimental conditions detailed in Table 2 and the figure legend, and shown for the first and second dilution sequences.

350 nm indicated an adsorption maximum at 262 nm, and single point measurements referenced to the solvent background were made in triplicate at this wavelength. Following Beer–Lambert's law the adsorbance, A_d, is given by $A_d = \varepsilon l C$, where ε is the molecular adsorption coefficient and l the sample path length. The solution concentrations were then obtained by comparison with a LAS-4 calibration curve, for factor 2 dilutions from 2 to 0.0625 mM.

EXPERIMENTAL RESULTS

For all the measurements made (experiments 1–5 in Table 2), the NR data are consistent with a monolayer of deuterated surfactant adsorbed at the interface, with a typical thickness ~20 Å. Each reflectivity profile is modeled by a thin layer of uniform composition to give a thickness, d, and a scattering length density, ρ. From this the area per molecule and the adsorbed amount are estimated using eq 2, and this represents an average over any lateral inhomogeneities.[20] The time-dependent adsorption was measured with relatively short measurement times, and typically the error in the area per molecule is ±5 Å^2, which translates to an error in the adsorbed concentration of $\pm 0.2 \times 10^{-6}$ mol m^{-2}. The LAS-4 adsorption at equilibrium was measured with a longer measurement time and is 55 ± 2 Å^2 ($\Gamma \sim 3.0 \pm 0.1 \times 10^{-6}$ mol m^{-2}).

From the time dependence of the adsorption data in Figure 5, the re-equilibration process can be seen to be relatively slow. In most cases it is longer than the time for the dilution to take place. Furthermore, the process depends upon the flow rate, the extent of the dilution (dilution factor), and the geometry of the flow cell.

MATHEMATICAL MODEL

Governing Equations. To gain a better understanding of the observed kinetics of desorption, a theoretical model that couples the fluid dynamics of the flow cell with the reaction, advection, diffusion, and adsorption of the surfactant is developed. A two-dimensional setup, as shown in Figure 6, is

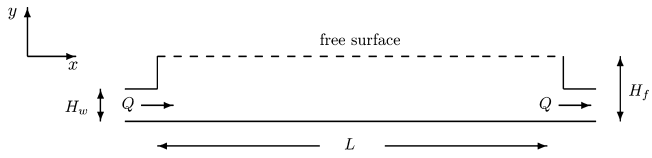

Figure 6. Schematic diagram of the flow cell.

assumed. The relevant parameters in the model, and their sizes, are given in Table 3. The Froude number, $Fr = U/(gH_f)^{1/2}$ (U, g, and H_f are defined in Table 3), for the experiment is typically 10^{-3}, and so the free surface is assumed to be effectively flat. In the model it is assumed that all micelles have the same aggregation number, N, and that micelles form according to the single-step reaction (see Breward and Howell[26])

$$NS \Leftrightarrow_{k_0^-}^{k_0^+} S_m \tag{3}$$

where $k_0^{\pm}$ are the rate constants for the aggregation/dissociation reactions.

The variables of the model are scaled appropriately to obtain a dimensionless model for the system; the corresponding dimensionless parameters that appear in the model are defined in Table 4.

The reduced Péclet number Pe^* is a ratio of the time scales for vertical diffusion and horizontal convection. The large values indicate that convection dominates the flow except in a boundary layer at the interface. The small values of the reduced Reynolds number Re^* confirm that laminar flow exists. The

dx.doi.org/10.1021/la304091g | Langmuir 2012, 28, 17339–17348

Table 3. Typical Parameters for Experiments 1−5[a]

parameter	description	range of values	units
S_T	total surfactant concentration	2	mol m^{-3}
S_{cmc}	critical micellar concentration	1.6	mol m^{-3}
S_E	monomer concentration in equilibrium	1.56	mol m^{-3}
Γ_{sat}	adsorbed saturation concentration	3.5×10^{-6}	mol m^{-2}
D_s	monomer diffusion coefficient	5.5×10^{-10}	m^2 s^{-1}
D_{sm}	micelle diffusion coefficient	1.5×10^{-10}	m^2 s^{-1}
D_Γ	surface diffusion coefficient	10^{-9}	m^2 s^{-1}
k	adsorption rate constant	0.19	mol m^{-3}
k_0^-	micelle dissociation rate constant	20	s^{-1}
H_f	height of fluid	$(2.7–6.9) \times 10^{-3}$	m
H_w	height of weir	$(1.5–3) \times 10^{-3}$	m
L	length of trough	$(70–216) \times 10^{-3}$	m
W_1	width of trough	50×10^{-3}	m
Q	dilution rate	$(1.0–4.2) \times 10^{-8}$	m^3 s^{-1}
U	mean horizontal velocity (Q/W_1H_f)	$(3–31) \times 10^{-4}$	ms^{-1}
ρ	density of water	10^3	kg m^3
μ	dynamic viscosity of water	10^{-3}	Pa s
γ_0	surface tension of water	7×10^{-2}	N m^{-1}
R	universal gas constant	8.31	J mol^{-1} K^{-1}
T	absolute temperature	298	K

[a]Parameter values are taken from refs 17, 23, 26−, and 28.

Table 4. Definitions of the Relevant Dimensionless Parameters and Corresponding Typical Values for Experiments 1−5

parameter	expression	description	value
ε	H_f/L	aspect ratio	$(1.3–9.9) \times 10^{-2}$
Re^*	$\varepsilon^2 UL\rho/\mu$	reduced Reynolds number	$(1–4.9) \times 10^{-2}$
Pe^*	$\varepsilon^2 UL/D_s$	reduced Péclet number	(19−89)
Ma	$RT\Gamma_{sat}/\mu U$	Marangoni number	$(2.8–28) \times 10^4$
λ_D	$\Gamma_{sat}/H_f S_{cmc}$	ratio of adsorbed to net surfactant conc.	$(3.2–8.1) \times 10^{-4}$
β	k/S_{cmc}	dimensionless Langmuir rate constant	0.12
S^*	S_T/S_{cmc}	dimensionless total surfactant conc.	1.25
S_0	S_E/S_{cmc}	dimensionless monomer equilibrium conc.	0.98
h_w	H_w/H_f	dimensionless weir height	(0.35−0.56)
K	$H_f^2 k_0^-/D_s$	dimensionless reaction rate constant	$(1.3–1.7) \times 10^5$
D	D_{sm}/D_s	ratio of diffusion coefficients	0.27
D^*	D_Γ/D_s	ratio of diffusion coefficients	1.8
N	−	micelle aggregation number	53

Marangoni number Ma is typically large, which implies that surface tension gradients dominate over viscous effects. Hence lateral variations in the surface adsorption will rapidly re-equilibrate. The large value of the dimensionless reaction rate constant K means that the surfactant monomer and micelles are in equilibrium in the bulk.

The velocity of the fluid, $\mathbf{u} = (u, v)$, and pressure p satisfy the dimensionless Navier−Stokes equations

$$u_x + v_y = 0 \tag{4}$$

$$Re^*(u_t + uu_x + vu_y) = -p_x + \varepsilon^2 u_{xx} + u_{yy} \tag{5}$$

$$\varepsilon^2 Re^*(v_t + uv_x + vv_y) = -p_y + \varepsilon^4 v_{xx} + \varepsilon^2 v_{yy} \tag{6}$$

where the subscripts x, y, and t define derivatives with respect to their variables, x and y represent horizontal and vertical coordinates as defined in Figure 3, and t represents time. The aspect ratio of the trough is defined by $\varepsilon = H_f/L$, and the reduced Reynolds number is defined by $Re^* = \varepsilon^2 UL\rho/\mu$. The concentration of surfactant monomers, micelles, and surface excess are denoted by S, S_m, and Γ, respectively. Following the mathematical model derivation of Breward and Howell,[26] S and S_m satisfy the reaction−advection−diffusion equations

$$Pe^*(S_t + uS_x + vS_y) = \varepsilon^2 S_{xx} + S_{yy} + K(S_m - S^N) \tag{7}$$

$$Pe^*(S_{mt} + uS_{mx} + vS_{my}) = D(\varepsilon^2 S_{mxx} + S_{myy}) - K(S_m - S^N) \tag{8}$$

in the bulk solution. Here $Pe^* = \varepsilon^2 UL/D_s$ is the reduced Péclet number, $D = D_{sm}/D_s$ is the dimensionless diffusivity for the micellar phase, and $K = H_f^2 k_0^-/D_s$ is the dimensionless rate constant for aggregation. Assuming that the surface concentration at the air−water interface is in thermodynamic equilibrium with the bulk, then Γ satisfies the Langmuir isotherm[4]

$$\Gamma = \left.\frac{S}{\beta + S}\right|_{y=1} \tag{9}$$

where $\beta = k/S_{cmc}$ is the dimensionless rate parameter for the Langmuir isotherm. At the air−water interface we assume that only monomers may adsorb, so the flux of micelles normal to the interface is zero

$$S_{my} = 0, \quad \text{on} \quad y = 1 \tag{10}$$

and the concentration of adsorbed surfactant, Γ, satisfies the conservation equation

$$-S_y = \lambda_D Pe^*(\Gamma_t + (u\Gamma)_x) - \varepsilon^2 \lambda_D D^* \Gamma_{xx}, \quad \text{on} \quad y = 1 \tag{11}$$

where $\lambda_D = \Gamma_{sat}/H_f S_{cmc}$ is the ratio of adsorbed surfactant to net surfactant concentration, and $D^* = D_\Gamma/D_s$ is the dimensionless surface diffusivity. The kinetic condition and tangential stress balance on the air−water interface give

$$v = 0, \quad \text{on} \quad y = 1 \tag{12}$$

$$u_y + \varepsilon^2 v_x = \gamma^* \gamma_x, \quad \text{on} \quad y = 1 \tag{13}$$

where γ denotes the dimensionless surface tension, $\gamma^* = \Delta\gamma H_f/\mu UL$, and $\Delta\gamma$ is the typical difference in surface tension across the air−water interface. Since the surface concentration at the air−water interface is in thermodynamic equilibrium with the bulk, then the surface tension, γ, can be related to the adsorbed concentration, Γ, via the Frumkin equation[4]

$$\gamma - \frac{\gamma_0}{\Delta\gamma} = \frac{\varepsilon Ma}{\gamma^*}\log(1 - \Gamma) \tag{14}$$

where $Ma = RT\Gamma_{sat}/\mu U$ is the Marangoni number. Differentiating eq 14 and substituting into eq 13 thus gives

dx.doi.org/10.1021/la304091g | Langmuir 2012, 28, 17339−17348

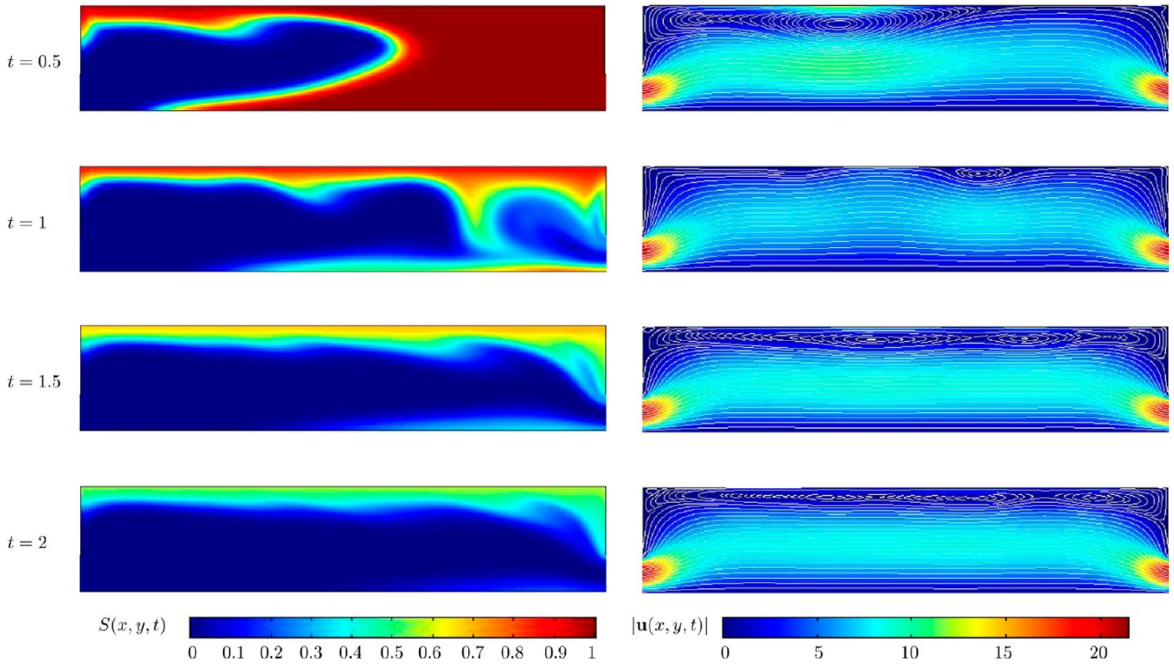

Figure 7. Plots of (a) surfactant concentration and (b) velocity profile and streamlines for Ma = 1000 and Pe^* = 75. The other parameters used are ε = 0.2, Re^* = 0.05, and $\lambda_D = 4 \times 10^{-4}$.

$$u_y + \varepsilon^2 v_x = -\varepsilon Ma \frac{\Gamma_x}{1-\Gamma}, \quad \text{on} \quad y = 1 \tag{15}$$

At the inlet we approximate the flow as follows

$$u = \frac{6}{h_w^3} y(h_w - y), \quad v = 0, \quad \text{on} \quad x = 0, \quad 0 < y < h_w \tag{16}$$

where h_w is the dimensionless weir height and, since the dilution uses water and not surfactant solution, the boundary conditions for the surfactant phases are

$$S = S_m = 0, \quad \text{on} \quad x = 0, \quad 0 < y < h_w \tag{17}$$

At the outlet the pressure is zero and the diffusive flux of surfactant out of the cell is assumed to be negligible, i.e.

$$p = S_x = S_{mx} = 0, \quad \text{on} \quad x = 1, \quad 0 < y < h_w \tag{18}$$

Finally, on the fixed walls of the trough the velocity satisfies the no-flow, no-slip boundary conditions, and, assuming there is negligible adsorption of surfactant onto the Teflon trough, then the no-flux boundary conditions for the surfactant phases are imposed

$$\mathbf{u} = 0, \quad \mathbf{n}\cdot\nabla S = \mathbf{n}\cdot\nabla S_m = 0 \tag{19}$$

for $(x, y) \in \{(x, y)$: $y = 0$, $0 < x < 1$, and $x = 0$, 1, $h_w < y < 1\}$, where $\mathbf{n}$ is the unit normal to the boundary. Initially the fluid is at rest and all the surfactant phases are in equilibrium; hence

$$\mathbf{u} = 0, \quad S = S_0, \quad S_m = S_0^N, \quad \Gamma = \frac{S_0}{\beta + S_0}, \quad \text{at} \quad t = 0 \tag{20}$$

where the equilibrium concentration of monomer, S_0, satisfies

$$S_0 + S_0^N + \lambda_D \frac{S_0}{\beta + S_0} = S^* \tag{21}$$

and $S^* = S_T/S_{cmc}$ is the dimensionless net concentration of surfactant.

Numerical Simulations. In this section, numerical simulations of the model obtained using the COMSOL Multiphysics software package are presented. For simplicity, it is assumed that the solution following dilution is submicellar; i.e., the bulk concentration is below the cmc. This assumption is valid as the bulk concentration initially is just above the cmc, $S^* \sim 1.25$, and will quickly become subcmc during the first dilution.

The actual Marangoni number Ma for the system is $\geq 10^4$ (see Table 4). However, for Marangoni numbers $\sim 10^3$ and larger, the system becomes insensitive to the actual value used and further increases in Ma just make the computation intractable. Figure 7 shows the surfactant concentration profile, $S(x, y, t)$, and the velocity profile given by $|\mathbf{u}(x, y, t)|$ at times t = 0.5, 1, 1.5, 2 for Ma = 1000 and Pe^* = 75. The plots of the concentration profile, $S(x, y, t)$, show the existence of "roll waves" that develop near the free surface and which dissipate as t increases. The presence of these roll waves is due to Marangoni effects, and they have a repeating structure similar to Marangoni-convection cells, which are typically present in steady-state problems with surface-tension gradients. Significantly, however, the observed convection cells are advected along the trough by the bulk flow as opposed to typical Marangoni-convection cells that are stationary. The existence of these roll waves can be justified as follows; as the bulk solution is diluted from the left there will be a local region where the bulk surfactant decreases and so the surface concentration is no longer in equilibrium with the bulk. Thus, adsorbed surfactant desorbs so that a local equilibrium between the bulk and the surface is established. This results in a concentration gradient in the adsorbed surfactant on the whole trough scale and so the surfactant on the surface tries to re-equilibrate with the bulk inducing a Marangoni flow at the surface. The plots of the velocity profile show the formation of Marangoni-convection-like cells near the free surface, which propagate along the

dx.doi.org/10.1021/la304091g | Langmuir 2012, 28, 17339−17348

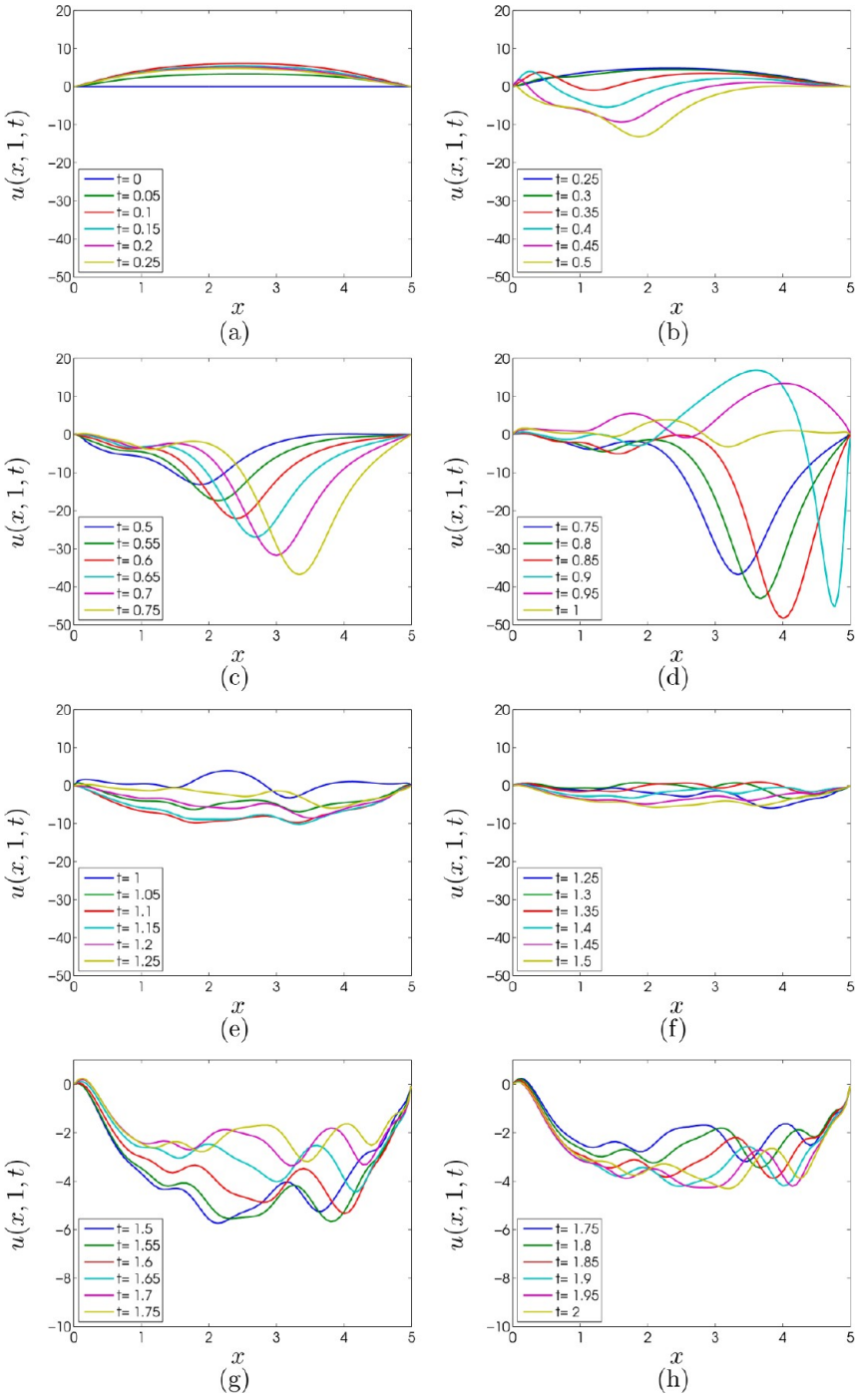

Figure 8. Plots of the surface velocity $u(x, 1, t)$ for different times during the dilution phase. Parameters used are $Ma = 1000$, $Pe^* = 75$, $\varepsilon = 0.2$, $Re^* = 0.05$, $\lambda_D = 4 \times 10^{-4}$, $D^* = 1.8$, $\beta = 0\ 12$, and $h_w = 0\ 35$.

trough and agree with the roll waves observed in the surfactant concentration profiles. The flow in the boundary layer on the trough base is approximately zero, and for $t \geq 1$ the boundary layer near $y = 1$ is also approximately stagnant. In the rest of the domain the flow profile tends to that of an approximate Poiseuille flow as t increases. Plots of the surface velocity $u = u(x, 1, t)$ in Figure 8 show that the surface flow is not unidirectional, which is in agreement with the observed Marangoni-convection-like cells, and reaches velocities that are up to five times the magnitude of that in the bulk.

Since the parameters ε, Re^*, $1/\varepsilon Ma$, λ_D, $1/Pe^*$, and $1/K$ are small, the structure of the solution to the model can be determined using asymptotic methods, and full details can be found in ref 29. The large Péclet number indicates that, away from the boundaries of the domain, diffusion can be neglected as the monomer and micellar phases are purely advected with the flow, as seen in Figure 7, where pure water injected from the left replaces the surfactant solution. Thus, after one volume exchange using the syringe pump, the concentration of surfactant away from the boundaries is effectively zero. Near the free surface, diffusion becomes important and boundary layers with dimensionless thickness $Pe^{*-1/2}$ form, and all the remaining surfactant will be confined to those layers.

dx.doi.org/10.1021/la304091g | *Langmuir* 2012, 28, 17339−17348

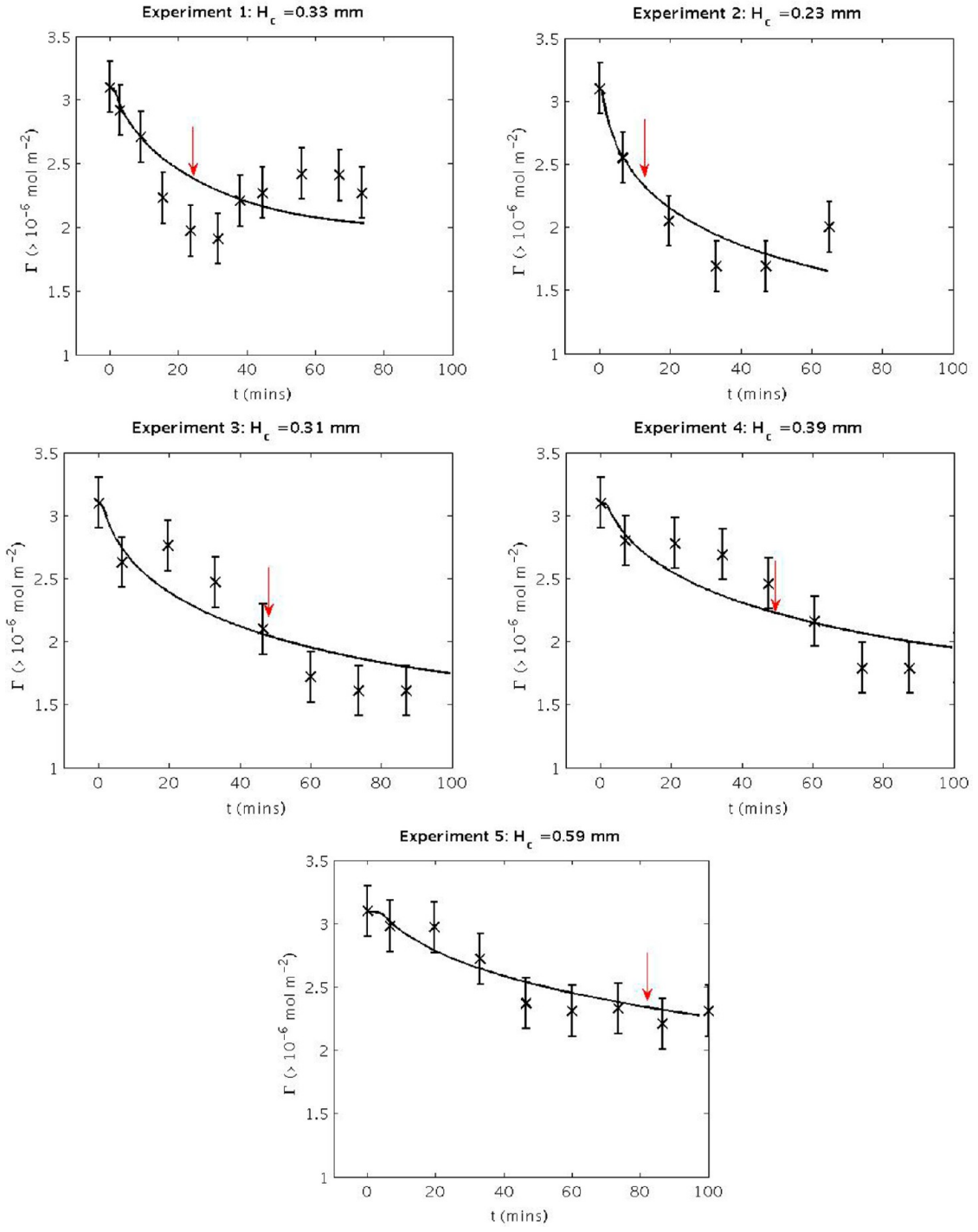

Figure 9. Comparison of the fitted diffusion-limited model (solid lines) with the NR data for the adsorbed concentration, $\Gamma(t)$, for the first dilution for experiments 1−5. The red arrow denotes the end of the dilution.

Diffusion-Limited Model. In order to simplify the model, the difference between the time scale for dilution and the time scale of the experiment is exploited. Assuming that the dilution occurs very quickly (and thus effectively instantaneously on the time scale of the experiment), a diffusion-limited model for the bulk surfactant phase, similar to that described by Tiberg et al.,[9,10] can be derived, in which there is no flow of liquid. Assuming that, before the dilution phase, the surfactant phases are in equilibrium with each other, then after the dilution has occurred there will be two distinct regions: one near the air−liquid interface where the surfactant phases are in equilibrium, which has (unknown) depth H_c, and one below where the bulk surfactant concentration is zero. Assuming no concentration variations in the x-direction, the dimensionless equations satisfied by S, S_m, and Γ become

$$S_t = S_{yy} + K(S_m - S^N) \tag{22}$$

$$S_{mt} = DS_{myy} - K(S_m - S^N) \tag{23}$$

with boundary conditions

dx.doi.org/10.1021/la304091g | Langmuir 2012, 28, 17339−17348

$$-S_y = \lambda_D \Gamma_t, \quad \Gamma = \frac{S}{\beta + S}, \quad S_{my} = 0, \quad \text{on} \quad y = 1 \tag{24}$$

$$S_y = S_{my} = 0, \quad \text{on} \quad y = 0 \tag{25}$$

and initial conditions

$$S(y, 0) = \begin{cases} 0, & 0 < y < 1 - H_c/H_f \\ S_0, & 1 - H_c/H_f \le y < 1 \end{cases} \tag{26}$$

$$S_m(y, 0) = \begin{cases} 0, & 0 < y < 1 - H_c/H_f \\ S_0{}^N, & 1 - H_c/H_f \le y < 1 \end{cases} \tag{27}$$

$$\Gamma(0) = \frac{S_0}{\beta + S_0} \tag{28}$$

where the monomer equilibrium concentration before the dilution, S_0, satisfies eq 21. The unknown dimensionless layer thickness H_c/H_f can then be used to fit the experimental data. The dimensionless rate parameter, K, is proportional to the micelle dissociation rate constant, k_0^-, whose value for LAS-4 is unknown. However, it is widely accepted that the time scale associated with dissociation is much quicker than the time scale for diffusion in the y-direction and hence $K \gg 1$. (Note that if K is assumed to be of order 1, then k_0^- must be of order 10^{-5} s^{-1}; i.e., the micelle dissociation time scale would be of the order of 24 h, which is clearly far greater than what is observed.) Furthermore, a typical value for k_0- for a 2.5 mol m^{-3} solution of C_{16}TAB obtained in ref 26 is 20 s^{-1}, which gives $K = 6.1 \times 10^5$ for the parameters associated with experiment 2. Thus, eqs 22−28 can be simplified by taking an asymptotic expansion of the variables S, S_m, and Γ for large K. Physically this corresponds to the equilibrium limit where $S_m \sim S^N$. Similarly, the problem can be simplified further since $\lambda_D \ll 1$, which physically corresponds to the concentration of the surface excess being negligible compared with the total bulk surfactant concentration. Hence, the model is reduced to a single partial differential equation for S

$$(S + S^N)_t = (S + DS^N)_{yy} \tag{29}$$

with boundary conditions

$$S_y = 0, \quad \text{on} \quad y = 0, 1 \tag{30}$$

and initial condition eq 27where S_0 now satisfies

$$S_0 + S_0^N = S^* \tag{31}$$

The micelle and adsorbed concentrations are given by

$$S_m = S^N, \quad \text{and} \quad \Gamma = \left.\frac{S}{\beta + S}\right|_{y=1} \tag{32}$$

respectively.

COMPARISON WITH MODEL AND DISCUSSION

Equations 22−32 are solved numerically using MATLAB's parabolic equation solver pdepe and via the method of least-squares to fit the unknown parameter H_c/H_f to the experimental data. The additional data point $\Gamma = 3.1 \times 10^{-6}$ mol m^{-2} (the equilibrium value for a 2 mM solution of LAS-4) is added at $t = 0$ to the observed experimental data. Plots of the adsorbed amount, Γ, against time are shown in Figure 9 and are in good agreement with the NR data from Figure 5 over the first dilution sequence.

The mathematical model reproduces well the experimental adsorption data, although there are regions where the adsorption fluctuates from the general trend. This is attributed to surface Marangoni effects, as illustrated in the plots of the COMSOL simulations shown in Figures 5 and 6. The time dependence of the adsorbed amount is reproduced using only a single adjustable parameter, H_c, that varies from ∼0.2 to ∼0.6 mm dependent upon the experimental conditions. In the analysis of the desorption of surfactants from hydrophilic and hydrophobic solid surfaces, Tiberg et al.[9,10] reported values ∼0.1 mm for the "stagnant layer" of their broadly similar model. However, they did not report any variations in that surface layer for different flow conditions.

The mathematical model presented here predicts that a plot of H_c/H_f against the reduced Péclet number, Pe^*, should scale as $Pe^{*-1/2}$, and this is shown in Figure 10. The solid curve in the figure is for $H_c/H_f = CPe^{*-1/2}$ with $C = 0.52$, which is in good agreement with the blue neutron data. This reinforces the earlier assertion of the leading-order asymptotic solution to the full model that there exists a diffusive boundary layer of order $Pe^{*-1/2}$ near the air−water interface. The red data points in Figure 10 are from estimates of the surface diffusion boundary layer obtained from determining the final solution concentration in the trough using UV adsorption spectroscopy for experiments 1−3. Although the variation in the data obtained from the solution composition is larger, the results are broadly consistent with the adsorption data. The differences reflect two factors: the greater uncertainty associated with the concentration measurements and the uncertainty when equilibrium is reached in the adsorption measurements.

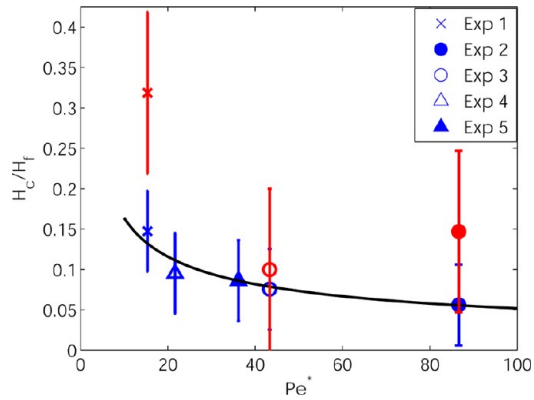

Figure 10. Comparison of the fitted dimensionless parameter H_c/H_f versus the reduced Péclet number, Pe^*, for the five different experimental conditions. The blue data points are from the NR data as described above, and the red data points are from a determination of the final surfactant concentration in the trough. The curve $H_c/H_f = CPe^{*-1/2}$ is denoted by the solid line, where $C = 0.52$ is obtained by fitting the blue neutron data only.

The model for the surface-desorption kinetics has three main assumptions: that a surface boundary layer exists, that the dilution of the subphase is rapid compared with the desorption process, and that the desorption is controlled by monomer diffusion. Both the COMSOL numerical simulations and the analysis of the adsorption data, and particularly the scaling of the surface boundary layer thickness with reduced Péclet number, provide strong evidence for the existence of a surface

dx.doi.org/10.1021/la304091g | Langmuir 2012, 28, 17339−17348

boundary layer. Although for some of the experimental conditions used the dilution process was not short compared with the desorption time scale, this does not seem to affect the interpretation of the data substantially. Hence it must be concluded that this is not a strong or overwhelming criterion.

The mathematical model was developed for surfactant solutions with bulk concentrations that can exceed the cmc, and so surfactant monomer and micelle diffusion and micelle dissolution are included. However, the numerical simulations using COMSOL assumed submicellar solutions. This assumption was justified on the grounds that the measurements were made for solutions initially only just above the cmc, and so the solutions would rapidly become subcmc on dilution. Hence it can be assumed that the surface kinetics to be dominated by monomer diffusion and that micelle diffusion and disassociation play only a secondary role here.

■ SUMMARY

The slow surface re-equilibration of surfactant at the air−water interface due to subphase dilution has been characterized by time-dependent neutron reflectivity under different flow conditions and geometries. The mathematical model developed for diffusion from a near-surface boundary layer provides a good description of the kinetic data. The dependence of the boundary layer depth on the reduced Péclet number shows that the desorption is controlled by the nature of the flow. This provides an important insight into the rinse mechanism, which may be applied to more realistic and practical situations.

■ AUTHOR INFORMATION

Corresponding Author

*E-mail address: jeff.penfold@stfc.ac.uk.

Notes

The authors declare no competing financial interest.

■ ACKNOWLEDGMENTS

ISIS is acknowledged for the beam time on INTER and STFC and EPSRC for the CASE award for C.E.M. C.J.W.B. and I.M.G. acknowledge Award No. KUK-C1-013-04, made by King Abdullah University of Science and Technology (KAUST), for support. The authors acknowledge P. Carroll, G. Lawton, and W. Ranken at Unilever, Port Sunlight, for the construction of the flow cell.

■ REFERENCES

(1) Noskov, B. Kinetics of adsorption from micellar solutions. *Adv. Colloid Interface Sci.* **2002**, *95*, 237.

(2) Lucassen, J. Adsorption kinetics in micellar solutions. *Faraday Discuss.* **1975**, *59*, 76.

(3) Fainerman, V. B. Kinetics of adsorption of ionic surfactants at the solution−air interface and the nature of the adsorption barrier. *Colloids Surf.* **1991**, *57*, 249.

(4) Chang, C. H.; Franses, E. I. Adsorption dynamics of surfactants at the air−water interface: A critical review of mathematical models, data, and mechanisms. *Colloids Surf.* **1995**, *100*, 1.

(5) Miller, R.; Joos, P.; Fainerman, V. B. Dynamic surface and interfacial tensions of surfactant and polymer solutions. *Adv. Colloid Interface Sci.* **1994**, *49*, 249.

(6) Eastoe, J.; Dalton, J. S. Dynamic surface tension and adsorption mechanisms of surfactants at the air−water interface. *Adv. Colloid Interface Sci.* **2000**, *85*, 103.

(7) Svitova, T. F.; Wetherbee, M. J.; Radke, C. J. Dynamics of surfactant sorption at the air−water interface: Continuous flow tensiometry. *J. Colloid Interface Sci.* **2003**, *261*, 170.

(8) Ferri, J. K.; Gorevski, N.; Kotsmar, C. S.; Leser, M. E.; Miller, R. Desorption kinetics at fluid interfaces by novel coaxial capillary pendant drop experiments. *Colloids Surf., A* **2008**, *319*, 13.

(9) Tiberg, F.; Jonsson, B.; Lindman, B. Ellipsometry studies on the self-assembly of nonionic surfactants at the silica−water interface: Kinetic aspects. *Langmuir* **1994**, *10*, 374.

(10) Tiberg, F. Physical characterization of nonionic surfactant layers adsorbed at the hydrophilic and hydrophobic solid surfaces by time-resolved ellipsometry. *J. Chem. Soc., Faraday Trans.* **1996**, *92*, 531.

(11) Valkovska, D. S.; Shearman, G. C.; Bain, C. D.; Darton, R. C.; Eastoe, J. Adsorption of ionic surfactants at an expanding air−water interface. *Langmuir* **2004**, *20*, 4436.

(12) Manning-Benson, S.; Bain, C. D.; Darton, R. C. Measurement of dynamic surface excess in an overflowing cylinder by ellipsometry. *J. Colloid Interface Sci.* **1997**, *189*, 109.

(13) Manning-Benson, S.; Parker, S. W.; Bain, C. D.; Penfold, J. Measurement of dynamic surface excess in an overflowing cylinder by neutron reflection. *Langmuir* **1998**, *14*, 990.

(14) Howell, P. D.; Breward, C. J. B. Mathematical modelling of the overflowing cylinder experiment. *J. Fluid Mech.* **2003**, *474*, 275.

(15) Ward, A. F. H.; Tordai, L. Time dependence of boundary tensions in solution. *J. Chem. Phys.* **1946**, *14*, 453.

(16) Diamant, H.; Ariel, G.; Andelman, D. Kinetics of surfactant adsorption: The free energy approach. *Colloids Surf., A* **2001**, *183−185*, 259.

(17) Phan, C. M.; Nguyen, A. V.; Evans, G. M. Dynamic adsorption of sodium dodecylbenzene sulfonate and dowfroth250 onto the air−water interface. *Mater. Eng.* **2005**, *18*, 599.

(18) Miller, C. A.; Raney, K. H. Solubilization−emulsification mechanisms of detergency. *Colloids Surf.. A* **1993**, *74*, 169.

(19) www.unilever.co.uk/sustainable-living/uslp/index.aspx

(20) Lu, J. R.; Thomas, R. K.; Penfold, J. Surfactant layers at the air−water interface: Structure and composition. *Adv. Colloid Interface Sci.* **2000**, *84*, 143.

(21) INTER reflectometer at the ISIS facility, http://www.isis.stfc.ac.uk/instruments/INTER/.

(22) Penfold, J.; Richardson, R. M.; Zarbakhsh, A.; Webster, J. R. P.; Bucknall, D. G.; Rennie, A. R.; Jones, R. A. L.; Cosgrove, T.; Thomas, R. K.; Higgins, J. S.; Fletcher, P. D. I.; Dickinson, E.; Roser, S. J.; McLure, I. A.; Hillman, A. R.; Richards, R. W.; Staples, E. J.; Burgess, A. N.; Simister, E. A.; White, J. W. Recent advances in the study of chemical surfaces and interfaces by specular neutron reflection. *J. Chem. Soc., Faraday Trans.* **1997**, *93*, 3899.

(23) Penfold., J.; Thomas, R. K.; Dong, C. C.; Tucker, I.; Metcalfe, K.; Golding, S. Equilibrium surface adsorption in complex anionic/nonionic surfactant mixtures. *Langmuir* **2007**, *23*, 10140.

(24) Thomas, R. K.; Golding S. *Private communication.*

(25) Ma, J. G.; Boyd, B. J.; Drummond, C. J. Positional isomers of linear sodium dodecyl benzene sulfonate: Solubility, self-assembly, and air−water interface activity. *Langmuir* **2006**, *22*, 8646.

(26) Breward, C.; Howell, P. D. H. Straining flow of a micellar surfactant solution. *Eur. J. Appl. Math.* **2004**, *15*, 511−531.

(27) Tucker, I.; Penfold, J.; Thomas, R.; Dong, C.; Golding, S.; Gibson, C.; Grillo, I. The variation in equilibrium surface adsorption behavior of alkylbenzene sulfonate surfactants using varying electrolyte concentrations. *Langmuir* **2011**, *27*, 6674−6682.

(28) Zhang, X. L.; Taylor, D. J. F.; Thomas, R. K.; Penfold, J. The role of polyelectrolyte on the adsorption of LAS at the air−water interface. *J. Colloid Interface Sci.* **2011**, *356*, 656−664.

(29) Morgan, C. E. D.Phil. Thesis, Oxford University, 2012.